Reef slope geometries and facies distribution: controlling factors(Messinian, SE Spain)

Jesús Reolid[1]
Christian Betzler[1]
Juan Carlos Braga[2]
José Manuel Martín[2]
Sebastian Lindhorst[1]
John J. G. Reijmer[3]

[1] Institut für Geologie, Universität Hamburg. Bundesstraße 55, 20146 Hamburg, Germany. e-mail: jesus.reolid@uni-hamburg.de

[2] Departamento de Estratigrafía y Paleontología, Universidad de Granada, Avenida Fuentenueva s/n, 18002 Granada, Spain.

[3] Department of Sedimentology and Marine Geology, VU University Amsterdam, De Boelelaan 1085, 1081 HV Amsterdam, The Netherlands.

Abstract

Sea-level fluctuations and changes in sediment grain size are widely thought to be the main factors controlling carbonate platform slope geometries. Two successive clinoform bodies from the Upper Miocene Cariatiz carbonate platform (SE Spain) were selected to analyse geometry and facies distribution in relation to sea-level oscillations. Facies occurring in these clinoform bodies are from top to bottom reef-framework, reef-framework debris, *Halimeda* breccia, *Halimeda* rudstone and bioclastic packstone, as well as siltstone and marl. Slope geometry and facies, composition and distribution, are significantly different in each clinoform body. These differences are the result of the interaction of several factors such as coral growth, in-situ slope carbonate production, rockfalls and sediment gravity flows, hemipelagic rain, reworking of reef-slope facies and siliciclastic input. Changes in accommodation were related to sea-level fluctuations and controlled the relative impact of these factors. A sea-level fall took place in the time between deposition of the selected clinoform bodies and changed the hydrographical conditions of the basin. These changes influenced the presence of *Halimeda* and the grain-size distribution, and consequently the slope geometries. Reef-slope geometry is not exclusively controlled by changes in grain size. The stabilization by organic binding is proposed to be a significant factor controlling the slope deposition.

Key words: carbonate platform; microfacies; *Halimeda*; organic binding; Miocene; clinoform

Introduction

Sea-level changes are reported as the main factor controlling productivity, reef-slope geometry and stacking patterns of clinoform bodies in carbonate platforms (Kendall and Schlager 1981; Bosellini 1984; Eberli and Ginsburg 1989; Pomar and Ward 1994). According to Kenter (1990), carbonate platform slope angles are also closely linked to the sediment grain size. This was expanded by Adams and Schlager (2000) and Schlager and Adams (2001) relating the geometry of the slope to the sediment type and consequently to the hydrodynamic energy. Schlager and Reijmer (2009) showed that the type of carbonate mud, i.e. loose needles vs. sand-sized mud clasts, also plays a role in determining the slope of clinoform bodies. In order to test the applicability of these models to Upper Miocene carbonate platforms, two successive clinoform bodies from the latest episodes of reef progradation were selected in the Cariatiz carbonate complex (SE Spain) to calibrate facies distribution and grain-size variations in relation to sea-level oscillations.

Messinian coral reefs are well exposed in the Neogene basins of the Betic Cordillera in southeastern Spain and have been the subject of extensive research (Esteban 1980; Dabrio et al. 1981; Dabrio et al. 1985; Riding et al. 1991; Martín and Braga 1994; Braga and Martín 1996; Esteban 1996; Franseen and Goldstein 1996; Cornée et al. 2004, Warrlich et al. 2005; Cuevas et al. 2007; Sánchez et al. 2007; Rodríguez-Tovar et al. 2013). The Cariatiz carbonate platform in the Sorbas Basin (Almería) in cross-section exhibits a progradational pattern with well-developed clinoform bodies. These clinoform bodies show a downslope decrease of grain size, from reef-framework blocks and breccia to fine-grained packstone, and a basinward thinning and flattening. This facies distribution was assumed to be static when performing architecture analyses of the carbonate platform showing the vertical shifts of reef-slope facies during reef progradation following sea-level oscillations (Braga and Martín 1996; Cuevas et al. 2007). Up to now, however, no attempts were made to study variations in components and fabrics in successive reef-slope clinoform bodies affected by relative sea-level changes.

Mapping of facies distribution, with the support of terrestrial LIDAR data and microfacies analysis, shows that the two selected clinoform bodies exhibit different slopes geometries and completely different facies distribution patterns. Changes in slope geometries are linked to changes in grain size and facies distribution. In the clinoform bodies, facies distribution is the result of the interaction of different factors related to carbonate production and its distribution along the reef slope. These factors seem to be linked to sea-level fluctuations. A sea-level fall appears as the main cause for facies variations in the studied clinoform bodies but it cannot completely explain reef-slope geometries. The aim of this research is to discuss the nature, importance and extent of all the factors affecting the geometry of clinoform bodies and to contribute to the ongoing discussion on carbonate slope systems and their controls.

Geological setting

The studied outcrop is located in the Barranco de los Castaños ravine near the village of Cariatiz, at the northern margin of the Sorbas Basin (SE Spain) (Fig. 1). The Sorbas Basin is elongated in an E–W direction, and is bound by metamorphic rocks from the Internal Betic Zone cropping out in the Sierra de los Filabres to the north and in the Sierra Alhamilla and Sierra Cabrera to the south.

The basin-fill is up to 700 m thick and consists of several stratigraphic units ranging from Middle Miocene to Quaternary in age (Martín and Braga 1994). These stratigraphic units are separated by unconformities (Fig. 2a). The Upper Tortonian Unit comprises neritic to deep-sea siliciclastics and carbonates (Kleverlaan 1989; Martín and Braga 1994). The overlying Azagador Member (Völk and Rondeel 1964) consists of platform packstone and bioclastic sandstone. Basinward, the Azagador Member grades into fine-grained packstone and marl of the Lower Abad Member (Martín and Braga 1994), deposited close to the Tortonian-Messinian boundary (Sierro et al. 1993). The lowest Messinian reef deposits constitute the Bioherm Unit (Martín and Braga 1994) which contains coral and algal bioherms among packstone background deposits grading basinward into silty marl and marl with intercalated diatomite. The unconformably overlying Messinian Fringing Reef Unit is the scope of this study. It comprises carbonate platform deposits and related basinal silty marl, marl and diatomite from the Upper Abad Member (Martín and Braga 1994). The southern end of the Barranco de los Castaños section is located at the transition from reef carbonates to basinal marl and silty marl (Fig 2a). A basin-wide erosional surface, with signs of subaerial exposure, bounds the top of the Fringing Reef Unit. The Upper Abad marl and the distal Fringing Reef deposits are onlapped by a series of evaporite, carbonate and siliciclastic deposits (Ruegg 1964, Riding et al. 1998, 1999).

In the carbonate platform of the Fringing Reef Unit, Riding et al. (1991) and Braga and Martín (1996) differentiated a series of facies belts. From the inner platform to the basin these are (Fig. 2b):

1) Lagoon. Deposits from this belt are parallel beds of packstone to rudstone with coral, coralline algal, foraminifera and mollusc remains. Siliciclastic grains also occur, usually mixed with carbonates. Small patches of the coral *Porites* occur near the reef crest at the outer margin of lagoon sediments. Lagoonal beds dip 3° to southwest (N216E).

2) Reef framework. Deposits from this belt are about 20 m thick including from bottom to top: (a) a Pinnacle Zone dominated by columnar *Porites* connected by bridges of laminar growths. Coral colonies are grouped in up to 15 m high pinnacles separated by areas of reef debris. *Porites* skeletons are covered by thin coralline algal-foraminiferal crusts overgrown by thick stromatolitic crusts. A bioclastic matrix fills in the remaining spaces. (b) A Thicket Zone with a framework similar to the Pinnacle Zone but with more lateral continuity of the coral growths; and (c) a Reef crest made up of *Porites* colonies with platy to irregular shape.

3) Reef slope. These deposits consist of three different facies belts including from upper to lower slope: (a) the reef-talus slope, immediately in front of the Pinnacle Zone, consists of a breccia made up of framework blocks (the size of which decreases downslope) with *Halimeda* plates, bivalves, serpulids and coralline algae. The proximal reef slope (b) with packstone and rudstone that are made up of coralline algae, serpulids and molluscs (*Halimeda* bioclasts can be locally abundant); and the distal reef slope (c), which consists of silty marl and mudstone to packstone intercalated with basinal marl and diatomite.

Reef-framework and reef-slope facies are arranged into depositional wedges thinning downslope and basinward (Fig. 2b). These wedges, here referred as clinoform bodies, represent different phases of reef growth. In the Cariatiz carbonate platform it is possible to identify distinct stacking patterns of the clinoform bodies starting with lowstand deposits recorded by inverted wedges, These deposits consist of onlapping rudstone with bivalves, serpulids and red algae. Inverted wedges are overlain by an aggrading systems tract and highstand systems tract followed by a downstepping-offlapping systems tract (Pomar and Ward 1994; Braga and Martín 1996). Along with this progradation of the reef system, facies shifts occurred in response to sea-level fluctuations.

Methods

The study of the reef-slope facies and architecture relies on detailed outcrop mapping of reef clinoform bodies. This mapping was performed using panoramic photomosaics of the best-exposed parts of the succession. The study was carried out over a distance of more than 1100 m along reef progradation, but this work focuses on the youngest part of the prograding carbonate platform, which is the most accessible. Two clinoform bodies were selected due to their good exposure. The different reef facies within the two clinoform bodies were described and sampled. A petrographic analysis of 43 thin-sections was conducted to identify microfacies and components. Polished slabs were additionally used for analysing large bioclasts, sedimentary fabrics and structures.

The quantification of slope dimensions and slope geometries of the selected clinoform bodies was achieved by laser scanning with an Optech Laser Imaging ILRIS 3D terrestrial LIDAR of the Institute for Geology at Hamburg University. LIDAR data were processed using 3D-Reconstructor (Gexcel). Bedding planes and facies limits were mapped in the digital model.

The resulting polylines were exported into Autocad for body-dimensions and slope-angle measurements. Autocad was also used for converting the 3D model into 2D by projecting the system onto a plane positioned parallel-to-progradation.

Results

Clinoform bodies in the Barranco de los Castaños are intercalated with inverted wedges and fan-delta deposits (Braga and Martín 1996), as shown in Fig. 3. This study is focused on the last episodes of reef advance, which include two clinoform bodies, herein defined as Clinoform Body 1 (CB 1) and Clinoform Body 2 (CB 2), separated by a conglomerate body (Fig. 4a). The detailed analysis shows the differences in clinoform body geometries (Fig. 4b). Diverse facies in the clinoform bodies are documented in Table 1. Facies distribution is shown in Fig. 4c.

Clinoform Body 1

This clinoform body is 80 m high. In the direction of progradation (N160E) it extends for nearly 200 m (Fig. 4b). According to Adams and Kenter (2014), this body has a concave-upward linear profile, including three segments with different angles. The upper segment comprises the upper reef-talus slope with an approximate inclination of 60°. The middle segment includes the lower reef-talus slope and the proximal reef slope with angles between 40° and 30°. The lower segment corresponds to the distal slope with angles between 15° and 10°.

The uppermost part of the body consists of a ~10 m thick package of reef-framework which has a lateral extension of 35 m in the direction of progradation. The main volume of preserved reef framework corresponds to the Pinnacle Zone (Fig. 5). The Thicket Zone and the Reef

Crest are only locally preserved. The reef-framework debris facies is 22 m thick. The size and the amount of the debris decrease downslope from the outermost reef framework (Fig. 4c). The reef-framework debris gradually changes into the reef-talus slope breccia (*Halimeda* breccia), which is approximately 20 m thick and spreads basinward 15 m from the last large blocks (Fig. 6a). Up to 1 mm thick and 6 to 10 mm long *Halimeda* plates usually make up more than 20 % of the rock (Fig. 6b). Plates are usually oriented subparallel to bedding but locally they accumulate in patches with a random orientation. Sediments are floatstone and rudstone with varying amounts of micritic matrix. Within the *Halimeda* breccia, some patches occur which are formed by serpulid-tube clusters and red algae in a micritic matrix (Fig. 6c).

The good exposure of this clinoform body allows the facies change to be traced from the reef-talus slope into the proximal reef slope, in a transition zone characterized by interdigitation of *Halimeda* breccia and *Halimeda* rudstone facies, involving a change in the degree of lithification (Fig. 6d). The change in the degree of lithification parallels the basinward decrease of patches of encrusting organisms. The *Halimeda* rudstone is bedded in the proximal reef slope. Beds range in thickness from 5 to 30 cm and are grouped into an up to 15 m thick package. Patches of oysters, with some articulated individuals, occur at the top of this interval.

The transition between the *Halimeda* rudstone and the basinal facies is gradual. It occurs in an area with an alternation of 5 - 10 cm thick *Halimeda* rudstone beds and 15 - 25 cm thick siltstone and marl (Fig. 7). Deposits in this part of the slope are bioturbated. Low-angle tabular cross lamination pointing upslope occurs in the *Halimeda* rudstone beds (Fig.7). The alternation of *Halimeda* rudstone and fine-grained beds in this area is a 15 m thick fining- and thickening-upward sequence. Siltstone and marl with diatomite layers appear at the top of this alternation. The upper boundary of this sequence is an erosional surface at the base of the conglomerate body. The upper beds are deformed by the loading effect of overlying decametre-scale CB 2 reef-framework blocks (Fig. 8).

Clinoform Body 2

Clinoform Body 2 has a height of nearly 80 m. In the direction of progradation (N160E) it extends for 170 m (Fig. 4b). This body has a concave-upward exponential profile, according to the scheme of Adams and Kenter (2014). The reef-slope angles are approximately 80° - 60° in the reef-talus slope, 45° - 30° in the proximal reef slope and 20° - 15° in the distal reef slope.

The uppermost part of CB 2 consists of a 10 m high reef framework (Fig. 5) with a lateral extension of 30 m in the direction of progradation. The preserved framework facies are similar to those in CB 1. The transition from the reef framework to the reef-talus slope is gradual. In the uppermost reef-talus slope facies, there are decametre- to metre-scale reef-framework blocks. The abundance of stick-like *Porites* colonies indicates that most of the reef-framework blocks are derived from the Pinnacle or Thicket Zones. Locally there are some patches with bioclastic rudstone to packstone made up of bivalves mostly preserved as molds of articulated valves, gastropods, brachiopods and coral fragments. The reef-framework debris spreads basinward for 60 m from the lower limit of the reef framework and to the proximal to distal reef slope (Fig. 4). The average thickness of this facies is approximately 17 m.

A bioclastic packstone (Fig. 6e) occurs at the transition from the proximal to the distal reef slope, where bedding is locally deformed by decametric reef-framework debris (Fig. 9). Between the large blocks there are also some metre- to centimetre-scale reef-framework blocks. In the distal reef slope, 20 cm thick siltstone and marl units are interbedded with 20-

30 cm thick bivalve packstone beds. Some layers, usually red to ochre in colour, are very rich in coralline algae represented by sand-sized fragments and minor rhodoliths up to 15 cm in size. The entire package of alternating siltstone-marl and bivalve packstone is up to 5 m thick. Marl contains pebbles of quartz, schist and serpentinite at the most distal reef slope. These deposits are in part intensely bioturbated (Fig. 6f).

Conglomerate body

CB 1 and CB 2 are separated by a 50-100 cm thick and 110 m wide conglomerate unit. The conglomerates comprise up to 20 cm large clasts of quartzite, micaschist, marble, amphibolite and serpentine, which are derived from the Betic basement in the Sierra de los Filabres to the North. Clasts are supported by a microconglomeratic to sandy matrix. This body spreads from the uppermost part of the CB 1 reef slope to the most distal (lowest) point of the studied section. The largest clasts are located in the upper part of the slope and grain size decreases downward where deposits change into sandstone, basinal siltstone and marl. The thickness of the conglomerate changes from 50 cm in the upper slope to 100 cm downslope. In the proximal to distal reef slope, CB 1 siltstone and marl occur above and below the conglomerate body. The conglomerate base is an erosional surface over the underlying siltstone and marl (Fig. 7).

Discussion

Facies interpretation

It is proposed that the facies distribution in the clinoform bodies is controlled by the effects of the interaction of several processes. These processes are: a) carbonate production, linked to coral-reef growth and in-situ skeletal generation at the reef slope; b) physical processes such as rock falls, downslope gravity flows and current reworking; and c) sediment input from suspension or continental supply.

Coral-reef growth

Reef growth is water-depth limited and therefore restricted to the uppermost part of the slope in the shallow part of the photic zone. *Porites* colonies were early encrusted by stromatolites which are volumetrically and structurally important components of the reef framework (Riding et al. 1991). The presence of these crusts was crucial to protect and enforce the relatively delicate *Porites* colonies. The early lithification by stromatolitic crusts is thought to have exerted some sort of control on the way reef-framework facies broke and detached as individual blocks. The reef framework was preferentially broken along the planes of weakness provided by the vertical *Porites* sticks and the horizontal, laminar coral growths (Riding et al. 1991).

In-situ slope carbonate production

Halimeda plates are the main component in the reef-slope facies. Their major occurrence is in the reef-talus slope. This has also been described from the Messinian Níjar carbonate complex (Fig. 1). Mankiewicz (1988) and Martín and Braga (1989) showed that the most abundant *Halimeda* algal production area was in the reef-talus slope. Reef-framework blocks located in the reef-talus slope were suggested as ideal substrates for *Halimeda* growth (Riding et al. 1991). *Halimeda* plates either accumulated in-situ or were exported downslope by sediment flows, forming parautochthonous to allochthonous accumulations. These accumulations were syndepositionally encrusted by microbial biofilms that precipitated micrite contributing to the early lithification of the deposits (Adams and Kenter 2014). This is similar to *Halimeda* mounds from the Bioherm Unit (Martín et al. 1997). The presence of isolated specimens and clusters of articulated oyster shells in life position, with encrusting serpulids and coralline red algae, indicates that the reef-talus slope was the main skeletal production area together with the reef framework.

Rockfalls and gravity flows

The Pinnacle and Thicket Zones at the base of the reef framework were areas of potential instability by slumping and sliding of the underlying unconsolidated sediment at the top of the reef slope (Riding et al. 1991). Under these conditions, the collapse of the reef framework originating rocks and debris falls was a frequent phenomenon at the reef front (Hime et al. 1992; Martinsen 1994; Drzewievcki and Simó 2002; Berra et al. 2007; Playton et al. 2010). This resulted in the accumulation of blocks and debris on the reef-talus slope. These accumulations occur as discrete tongues (Playton et al. 2010). These tongues reach metre thickness in CB 1 and decametre thickness in CB 2. Rockfalls and debris falls involved the sediment produced on the reef-talus slope and triggered sediment flows spreading basinward to the distal reef slope. The transport capacity of these sediment flows decayed with increasing distance from the uppermost part of the slope (Adams et al. 1998). The progressive energy decrease in these sediment gravity flows as they moved down slope is proposed to control the grain-size reduction which occurs in the reef-slope sediments.

Hemipelagic rain

The abundance of siltstone and marl in the distal reef slope reflects the prevalence of deposition from suspension under quiet-water conditions (Drzewievcki and Simó 2002). Quiet-water conditions are also indicated by the extensive bioturbation of the distal reef-slope deposits. Thin diatomite layers in the basinal sectors are interpreted as the suspension fall-out of planktic-diatom blooms (Saint Martin et al. 2001).

Reworking of reef-slope facies

The presence of climbing-slope cross lamination in the distal reef slope points toward the existence of upslope directed northward-flowing bottom currents at the distal reef slope. These upslope currents were not acting continuously as cross-laminated coarse sediment alternates with bioturbated siltstone and marl. The change from cross lamination in CB 1 to parallel lamination in CB 2 suggests that bottom currents became less significant through time.

Siliciclastic input

The advance of the conglomerate body to the south is coeval with the continuous input of hemipelagic rain. This resulted in the mixture of terrigenous grains and basinal sediments in the distal reef slope. Braga and Martín (1996) identified this conglomerate as part of the middle-fan facies of a fan delta prograding southward from the Sierra de los Filabres and juxtaposed to the reef at some points.

Clinoform development and sea-level change

The facies distribution and depositional geometries along the 1100 m Cariatiz carbonate platform section reveal that a long-term cycle of relative sea-level rise and fall took place throughout reef advance (Braga and Martin 1996; Cuevas-Castell et al. 2007). According to Braga and Martín (1996) and Rodríguez-Tovar et al. (2013) the relative sea-level cycles reflect glacio-eustatic sea-level changes, as tectonic oscillations of the substrate can be discarded. Obliquity and precession controlled sea-level fluctuations are superimposed onto this general long-term trend (Rodríguez-Tovar et al. 2013). Precessional cycles (C2 cyclicity of Braga and Martín 1996; and RGP in Cuevas-Castell et al. 2007) are separated by lowstand deposits represented by the inverted wedges. Clinoform bodies reflect a higher-frequency cyclicity within the precessional cycles.

CB 1 occurs at the beginning of a sea-level fall in the last precession-forced cycle of the Cariatiz carbonate platform (C2.7 in Braga and Martín 1996; and RGP 8 in Cuevas-Castell et al. 2007). Rockfalls, in-situ carbonate production, gravity flows and hemipelagic rain were the main processes controlling facies distribution (Fig. 10a). Despite the relative sea-level fall and the decreasing accommodation space, the reef slope was large enough for the development of different subenvironments and successive facies belts, as in the examples shown by Adams et al. (1998, 2004) and Playton et al. (2010). At the distal reef slope, hemipelagic rain and upslope-directed bottom currents were the factors controlling the facies distribution. The occurrence of upslope-directed bottom currents alternates with quiet periods of basinal deposition (Fig. 10b). There was a period of bottom current inactivity recorded by bioturbated siltstone and marl during the last stages of development of CB 1.The conglomerates reached the reef slope while the siltstone and marl accumulated in the basin (Fig. 8).

A significant sea-level fall marked the end of CB 1 and the beginning of CB 2 development. This sea-level fall caused a major exposure of CB 1, which resulted in increasing erosion and breakage of CB 1 reef-framework. Rockfalls dominated the sedimentation and reef-framework debris piled up on the CB 1 reef slope (Fig. 10c). The upper part of the reef-framework debris is the substrate, where CB 2 reef-framework developed. As a result of a lower sea level this new reef framework grew downslope with respect to the position of reef growth in CB 1. The downstepping trend of the reef-framework base (Fig. 4c) indicates a continuous sea-level fall during the development of CB 2, whereas the accommodation during CB 1 formation was enough to allow for a classical reef-slope facies partitioning. This was significantly reduced in CB 2 where the facies distribution exhibits a completely different pattern. The proximity of the source area of the debris and a shorter reef slope did not allow for an adequate energy decay (Schlager and Adams 2001), and the reef-framework debris could be more easily exported, spreading down to the distal reef slope (Fig. 10d). Facies distribution at the distal reef slope therefore was controlled by sediment gravity flows and eventual rockfalls (Fig. 10e). These sediment gravity flows resulted in well-laminated bioclastic packstone in the distal reef slope. Hemipelagic rain affected the distal reef slope but was less significant than in CB 1.

Composition and sea-level change

Halimeda is a major component in CB 1 and is absent, or almost absent, in CB 2. In general, the facies with high concentrations of *Halimeda* (*Halimeda* breccia and *Halimeda* rudstone) are common in most of the Cariatiz reef-slope deposits including CB 1. The amount of *Halimeda* algae in reef-slope facies increased during reef progradation reaching its maximum value during the highstand and beginning of sea-level fall of the last precession-forced cycle (C2.7 of Braga and Martín 1996).

Facies with a high proportion of *Halimeda* plates also occur in other Messinian carbonate platforms (Esteban 1980; Mankiewicz 1988; Franseen and Mankiewicz 1991; Braga et al. 1996; Franseen and Goldstein 1996; Martín et al. 1997). Most of the Messinian *Halimeda* facies are found in the coral-bearing fringing-reef slope. *Halimeda* was also the main constituent in some bioherms located on non-rimmed platform slopes as in the bioherms described by Martín et al. (1997). Widespread and extensive *Halimeda* growth needs a relatively high nutrient environment (Drew and Abel 1983; Franseen and Mankiewicz 1991; Martín et al. 1997), which can ultimately be related to upwelling currents (Mankiewicz 1988).

Sánchez-Almazo et al. (2007) described stable oxygen and carbon isotope variations in shells of benthic and planktic foraminifera from the distal reef slope and basinal deposits adjacent to the analysed Cariatiz carbonate platform. In deposits laterally equivalent to CB 1, planktic and benthic $\delta^{13}C$ values are different, which was interpreted to reflect a pronounced water-stratification. Up-section, in deposits coeval to CB 2, the carbon isotope signals converge. According to Sánchez-Almazo et al. (2007) this indicates an important nutrient-content decrease and the disappearance of water stratification as a result of the mixing of deeper and shallower water masses.

This change in water stratification can be linked to the falling sea level during the last precession-forced cycle (Sánchez-Almazo et al. 2007). Gill and Clarke (1974) related the occurrence of upwelling in modern equatorial areas to sea-level fluctuations: upwelling takes place in stratified-water conditions during sea-level rise and highstand. Therefore, it is proposed that upwelling of nutrient-rich waters during sea-level rise and highstand stages also promoted the flourishing of *Halimeda* in the analysed carbonate platform. These upwelling conditions persisted at the beginning of sea-level fall in the last precession-forced cycle, as recorded by the presence of *Halimeda* breccia and *Halimeda* rudstone facies in CB 1. This is corroborated by upslope-pointing, low-angle cross lamination indicating the occurrence of upslope-directed bottom currents at the CB 1 distal reef slope. The decreasing water depth with continued sea-level fall finally caused water mixing and consequently the interruption of upwelling. The end of upwelling conditions probably explains the absence of *Halimeda* algae in CB 2 facies.

Geometry of clinoform bodies

The factors that control the geometry of carbonate platform slopes are summarized in Schlager (2005). These are the volume of sediment and platform height (Schlager 1981), the grain size (Kirkby 1987), and the erosion-deposition balance (Schlager and Camber 1986).

Schlager (1981) pointed out that the volume of sediment must decrease with decreasing height of the platform to keep the same geometry of the slope. At the studied section, platform height changed as a response to falling sea level, but the volume of sediment, as deduced from clinoform body size (Fig. 4), does not varies significantly from CB 1 to CB 2. The variation in the platform height from CB 1 to CB 2 seems to be more significant for changing the erosion-deposition balance and, consequently, facies distribution. Schlager and Camber (1986) described variations in slope geometries as a result of changes in the erosion-deposition balance during slope evolution. Erosional and depositional processes, as described in the previous section, were approximately the same in both clinoform bodies but acted with different intensity. Depositional processes are dominant during CB 1 formation while erosion is more relevant in CB 2, at least during the first stages of clinoform body development. Changes in the erosion-deposition balance therefore explain the different facies distribution, but not CB 1 and CB 2 geometries. Kirkby (1987) suggested that grain size controls the angle of stability of the slope. Our study shows that facies, and subsequently grain-size patterns, are completely different in each segment of the linear slope of CB 1, explaining changes in angles of these segments. These slope-angle changes related to grain size are also recorded in the transition from reef-framework debris to bioclastic packstone and basinal deposits in CB 2.

Adams and Kenter (2014) proposed additional factors controlling the steep angles in carbonate slopes. The major factors are the response to higher shear strengths in fine-grained carbonate slope sediments (Kenter 1990; Kenter et al. 2005; Schlager 2005; Playton et al. 2010), processes of early lithification and cementation of the slope sediments, and in-situ carbonate production and stabilization (Kenter 1990; Della Porta et al. 2003, 2004; Kenter et al. 2005).

Several factors contribute to the studied clinoform geometries in Barranco de los Castaños. In CB 1, with a linear profile, the different slope segments are characterized by different facies, with different grain-sizes, and consequently different angles of repose (Kenter 1990; Adams and Schlager 2000). The uppermost segment consists of an accumulation of reef-framework debris. The large debris blocks were nearly deposited in-situ and their imbrication allowed the high angle accumulation of 60°. The slope angles of 40° - 30° in the proximal and 15° - 10° in the distal reef slope correspond to the angles of repose of sand-gravel and mud respectively (Kenter 1990). Although these angles of repose are theoretically possible, field and seismic examples usually show lower angles than those described for CB 1 (see table 1 in Kenter 1990; and Adams and Schlager 2000).

Carbonates slopes with angles steeper than 30° - 45°, as in the studied section, were described by Kenter (1990) as the result of stabilization by organic framebuilding or by early lithification. That is the case of CB 1, where patches of serpulids and red algae as well as the abundant microbial micrite matrix and micritic envelopes in most of the bioclasts definitely contributed to the stabilization of the steep reef slope. This binding favoured the sediment accumulation in such steep angles of repose (Adams and Kenter 2014). Stabilization by microbial micrite was also suggested as an important factor controlling slopes geometries in Palaeozoic and Triassic platforms (Keim and Schlager 2001; Della Porta et al. 2003, 2004; Kenter et al. 2005; Schlager and Reijmer 2009). In these platforms, organic binding is more significant than grain size to determine the slope geometry.

In CB 2, decametric reef-framework blocks are the main component of the reef slope. The accumulation of blocks at the base of CB 2 occurred on top of the inherited CB 1 steep reef slope. The imbrication of such large blocks and the development of reef framework on top contributed to stabilize the reef slope despite its high angle. When the steep slope collapsed, reef debris reached the proximal to distal reef slope (Adams and Kenter 2014). Inheritance of substrate topography was suggested by Franseen and Goldstein (1996) as the dominant factor controlling slope geometries in Messinian reefs in the Molata de las Negras, coeval with the Cariatiz reef.

Conclusions

Two clinoform bodies, CB 1 and CB 2, were studied in the Messinian carbonate platform of Cariatiz. CB 1 has a concave-upward linear slope with facies represented by reef framework, reef-framework debris and *Halimeda* breccia in the reef-talus slope deposits. A *Halimeda* rudstone characterizes the proximal reef slope, and bioclastic packstone together with siltstone and marl the distal reef slope. Microbial micrite and micritic envelopes are common in this clinoform body. CB 2 has an exponential profile and its facies consist of reef framework, reef-framework debris from the reef-talus to distal reef slope, and bioclastic packstone and hemipelagic sediment in the distal reef slope.

This facies distribution is the response to the interaction of coral reef growth, in-situ slope carbonate production, rockfalls, sediment gravity flows, hemipelagic rain, reworking of reef-slope facies and siliciclastic input from the basement cropping out to the north. Changes in accommodation space, ultimately related to sea-level fluctuations, controlled the relative impact of these processes as well as their intensity, and, in this respect the type of sediment that finally accumulated along the reef slope. The vertical shift of facies shows that a sea-level fall took place from CB 1 to CB 2. This sea-level fall also changed the hydrographical conditions of the basin eliminating water stratification and upwelling, which prevailed during formation of CB 1 and promoted the abundance of *Halimeda* algae that do not occur in CB 2.

Facies distribution and changes in grain size are widely thought to be the main factors controlling slope geometries. However, geometry and facies analysis of CB 1 and CB 2 suggest that additional factors are needed to explain the steep angles of these slopes. The presence of microbial micrite, micritic envelopes and patches of encrusting organisms such as red algae and serpulids in CB 1 stabilized the steep angle of the reef slope. In CB 2, the heavy decametric reef-framework blocks deposited on top of an inherited, steep, prior topography were fixed there by the reef framework that settled and grew on top of them.

This study propose two new considerations to the ongoing discussion on carbonate slope systems: a) The dynamic behaviour of slope-facies changes related to sea-level fluctuations, in contrast with the classic static models; and b) the importance of organic binding in Neogene reef-slope geometries, similar to Palaeozoic and Triassic examples.

Acknowledgements

JR, CB and SL thank the Deutsche Forschungsgemeinschaft for financial support through the grant Be 1272/21-1 (NEOCARPS). JCB and JMM were funded through the project CGL2010-20857 of Ministerio de Ciencia e Innovación of Spain. JR thanks the VU-SMG Industrial Associates Programme for additional support. All the authors want to thank editor Prof. Maurice Tucker and reviewer Dr. Erwin Adams for their very valuable suggestions and comments which helped us to improve this paper.

References

Adams EW, Schlager W, Wattel E (1998) Submarine slopes with an exponential curvature. Sedimentary Geology 117:135–141

Adams EW, Schlager W (2000) Basic types of submarine slope curvature. Journal of Sedimentary Research 70:814–828

Adams EW, Schröder S, Grotzinger JP, McCormick DS (2004) Digital reconstruction and stratigraphic evolution of a microbial-dominated, isolated carbonate platform (Terminal Proterozoic, Nama group, Namibia). Journal of Sedimentary Research 74:479–497

Adams EW, Kenter JAM (2014) So different, yet so similar: comparing and contrasting siliciclastic and carbonate slopes. In: Verwer K, Playton TE, Harris PM (eds). Deposits, Architecture and Controls of Carbonate Margin, Slope and Basinal Settings. SEPM Special Publication 105, pp 14–25

Berra F (2007) Sedimentation in shallow to deep water carbonate environments across a sequence boundary: effects of a fall in sea-level on the evolution of a carbonate system (Ladinian-Carnian, eastern Lombardy, Italy). Sedimentology 54:721–735

Bosellini A (1984) Progradation geometries of carbonate platforms: examples from the Triassic of the Dolomites, northern Italy. Sedimentology 31:l–24

Braga JC, Martín JM (1996) Geometries of reef advance in response to relative sea-level changes in a Messinian (uppermost Miocene) fringing reef (Cariatiz reef, Sorbas Basin, SE Spain). Sedimentary Geology 107:61–81

Braga JC, Martín JM, Riding R, (1996) Internal structure of segment reefs: *Halimeda* algal mounds in the Mediterranean Miocene. Geology 24:35–38

Cornée JJ, Saint Martin JP, Conesa G, Münch P, André, JP, Saint Martin S, Roger S (2004) Correlations and sequence stratigraphic model for Messinian carbonate platforms of the Western and central Mediterranean. International Journal of Earth Sciences 93:621–633

Cuevas JM, Betzler C, Rössler J, Hüssner H, Peinl M (2007) Integrating outcrop data and forward computer modelling to unravel the development of a Messinian carbonate platform in SE Spain (Sorbas Basin). Sedimentology 54:423–441

Dabrio CJ, Esteban M, Martín JM (1981) The coral reef of Níjar, Messinian (uppermost Miocene), Almería Province, S.E. Spain. Journal of Sedimentary Petrology 51:521–539

Dabrio CJ, Martín JM, Megías AG (1985) The tectosedimentary evolution of Mio-Pliocene reefs in the province of Almería (SE Spain). In: Milá MD, Rosell J (eds). Sixth European Regional Meeting of the International Association of Sedimentologists, Excursion guidebook, pp 269-305

Della Porta G, Kenter JAM, Bahamonde JR, Immenhauser A, Villa E(2003) Microbial boundstone dominated carbonate slope (Upper Carboniferous, N Spain): microfacies, lithofacies distribution and stratal geometry. Facies 49:175–208

Della Porta G, Kenter JAM, Bahamonde JR (2004) Depositional facies and stratal geometry of an Upper Carboniferous prograding and aggrading high-relief carbonate platform (Cantabrian Mountains, N Spain). Sedimentology 51:267–295

Drew EA, Abel KM (1983) Growth of *Halimeda* in reefal and inter- reefal environments. In: Baker JT, Carter RM, Sammarco PW, Stark KP (eds). Proceedings, Great Barrier Reef Conference, pp 299 –304

Drzewiecki PA, Simó JA (2002) Depositional processes, triggering mechanisms and sediment composition of carbonate gravity flow deposits: examples from the Late Cretaceous of the south-central Pyrenees, Spain. Sedimentary Geology 146:155–189

Eberli GP, Ginsburg RN (1989) Cenozoic progradation of northwestern Great Bahama Bank, record of lateral platform growth and sea-level fluctuations. In: Crevello PD, Wilson JL, Sarg JF, Read JF (eds). Controls on Carbonate Platform and Basin Development. SEPM Special Publication 44, pp 339 –354

Esteban M, (1980) Significance of the Upper Miocene coral reefs of the Western Mediterranean. Palaeogeography, Palaeoclimatology, Palaeoecology 29:169 –188

Esteban M (1996) An overview of Miocene reefs from Mediterranean areas: general trends and facies models. Models for Carbonate Stratigraphy from Miocene Reef Complexes of Mediterranean Regions, SEPM Concepts in Sedimentology and Paleontology 5:3–53

Franseen EK, Mankiewicz C (1991) Depositional sequences and correlation of middle (?) to late Miocene carbonate complexes, Las Negras and Níjar areas, southeastern Spain. Sedimentology 38:871–898

Franseen EK, Goldstein RH (1996) Paleoslope, sea-level and climate controls on upper Miocene platform evolution, Las Negras area, Southeastern Spain. Models for Carbonate

Stratigraphy from Miocene Reef Complexes of Mediterranean Regions, SEPM Concepts in Sedimentology and Paleontology 5:159–176

Gill AE, Clarke AJ (1974) Wind-induced upwelling, coastal currents, and sea level changes. Deep-Sea Research 21:325–345

Hine AC, Locker SD, Tedesco LP, Mullins HT, Hallock P, Belknap DF, Gonzales JL, Neumann AC, Snyder SW (1992) Megabreccia shedding from modern, low relief carbonate platforms, Nicaraguan Rise. Geological Society of America Bulletin 104: 928–943

Kendall CGSC, Schlager W (1981) Carbonates and relative changes in sea-level. Marine Geology 44:181–212

Kenter JAM (1990) Carbonate platform flanks: Slope angle and sediment fabric. Sedimentology 72:777–794

Kenter JAM, Harris PM, Della Porta G (2005) Steep microbial boundstone-dominated platform margins - examples and implications. Sedimentary Geology 178:5–30

Keim L, Schlager W (2001) Quantitative compositional analysis of a Triassic carbonate platform (Southern Alps, Italy). Sedimentary Geology 139: 261–283

Kirkby MJ (1987) General models of long-term slope evolution through mass movement. In: Anderson MG, Richards KS (eds). Slope Stability, Geotechnical Engineering and Geomorphology. Wiley, London pp 359–379

Kleverlaan K (1989) Three distinctive feeder-lobe systems within one time slice of the Tortonian Tabernas fan, SE Spain. Sedimentology 36:25–45

Mankiewicz C, (1988) Occurrence and paleocologic significance of *Halimeda* in late Miocene reefs, Southeastern Spain. Coral Reefs 6:271–279

Martín JM, Braga JC (1989) Arrecifes Messinienses de Almería. Tipologías de crecimiento, posición estratigráfica y relación con las evaporitas. Geogaceta 7:66–68

Martín JM, Braga JC (1994) Messinian events in the Sorbas Basin in the Southeastern Spain and their implications in the recent history of the Mediterranean. Sedimentary Geology 90:257–268

Martín JM, Braga JC, Riding R (1997) Late Miocene *Halimeda* alga-microbial segments reefs in the marginal Mediterranean Sorbas Basin, Spain. Sedimentology 44:441–456

Martinsen O (1994). Mass movements. In: Maltman, A. (eds). The Geological Deformation of Sediments. Chapman & Hall, London, pp 127–165

Playton TE, Janson X, Kerans C (2010) Carbonate slopes. In: James NP, Dalrymple RW (eds). Facies Models 4, GEOtext 6: Geological Association of Canada, St John's, Newfoundland. pp 449–476

Pomar L, Ward WC (1994) Response of a late Miocene Mediterranean reef platform to high-frequency eustasy. Geology 22:131–134

Riding R, Martín JM, Braga JC (1991) Coral stromatolite reef framework, Upper Miocene, Almería, Spain. Sedimentology 38:799–818

Rodríguez-Tovar FJ, Sánchez-Almazo I, Pardo-Igúzquiza E, Braga JC, Martín JM (2013) Incidence of obliquity and precession-forced Milankovitch cycles in the western Mediterranean: early Messinian sedimentation in the Sorbas Basin (Almería, Southern Spain) International Journal of Earth Sciences (Geol Rundsch) 102:1735–1755

Ruegg GJH (1964) Geologische onderzoekingen in het bekken van Sorbas, S.E. Spanje. Geological Institute, University of Amsterdam, Amsterdam, Holland, pp 64

Saint Martin JP, Pestrea S, Conesa G (2001) Messinian diatom assemblages of infra-gypsum diatomites in the Sorbas basin (SE Spain). Cryptogamie Algology 22:127–149

Sánchez-Almazo IM, Braga JC, Dinarès-Turell J, Martín JM, Spiro B (2007) Palaeoceanographic controls on reef deposition: the Messinian Cariatiz reef (Sorbas Basin, Almería, SE Spain) Sedimentology 54:637–660

Schlager W (1981) The paradox of drowned reefs and carbonate platforms. Geological Society of America 92:197–211

Schlager W, Camber O (1986) Submarine slope angles, drowning unconformities, and self-erosion of limestone escarpments. Geology 14:762–765

Schlager W, Adams EW (2001) Model for the sigmoidal curvature of submarine slopes. Geology 29:883–886

Schlager W (2005) Carbonate sedimentology and sequence stratigraphy. SEPM Concepts in Sedimentology and Paleontology 8. SEPM (Society for Sedimentary Geology), Tulsa, pp 200

Schlager W, Reijmer JJG (2009) Carbonate platform slopes of the Alpine Triassic and the Neogene – a comparison. Austrian Journal of Earth Sciences 102:4–14.

Sierro FJ, Flores JA, Civis J, González-Delgado JA, Francés G (1993) Late Miocene globorotaliid event-stratigraphy and biogeography in the NE-Atlantic and Mediterranean. Marine Micropaleontology 21:143–168

Völk HR, Rondeel HE (1964) Zur Gliederung des Jungtertiärs im Becken von Vera, Südost-Spanien. Geologie en Mijnbouw 43:310–315

Warrlich G, Bosence D, Waltham D (2005) 3D and 4D controls on carbonate depositional systems: sedimentological and sequence stratigraphic analysis of an attached carbonate platform and atoll (Miocene, Níjar Basin, SE Spain). Sedimentology 52:363–389

Figure caption

Fig. 1 Regional setting of the Sorbas Basin and the Cariatiz Reef in SE Spain (modified from Braga and Martín 1996)

Fig. 2 a Neogene lithostratigraphy of the Sorbas Basin (modified from Sánchez-Almazo et al. 2007); **b** facies model for the Cariatiz fringing reef (after Riding et al. 1991 and Braga and Martín 1996)

Fig. 3 Barranco de los Castaños section, IW= Inverted wedges (modified from Braga and Martín 1996). Numbers indicate location of outcrops shown in the corresponding figures.

Fig. 4 a 3D model (point cloud) of studied clinoform bodies in Barranco de los Castaños section; **b** 2D projection of main surfaces, external and internal bedding, onto a plane oriented parallel to the progradation direction (N160E); **c** Facies distribution in CB 1 and CB 2

Fig. 5 *Porites* with vertical growth forms in the reef-framework facies. Example is from CB 2 (1 m scale bar)

Fig. 6 Barranco de los Castaños facies: **a** centimetric framework debris in the *Halimeda* breccia; **b** microscope view of *Halimeda* plates embedded in microbial micrite in the *Halimeda* breccia; **c** red algal nodule and serpulid clusters from patches within the *Halimeda* breccia; **d** outcrop view of *Halimeda* rudstone; **e** bivalve accumulation in the bioclastic packstone; and **f** bioturbated siltstone and marl. Scales: white bar = 2 mm; black bar = 2 cm

Fig. 7 a Outcrop view of the alternation of cross-laminated *Halimeda* rudstone beds with bioturbated marl beds in the distal reef slope of CB 1; **b** sedimentary structures interpreted over the outcrop view

Fig.8 a Outcrop view of the conglomerate body intercalated between CB 1 and CB 2; **b** facies interpretation of the outcrop view with conglomerate body (gray) among basinal sediments (yellow). The conglomerate erosional base cuts diatomite-rich beds (white) and basinal siltstone and marl. The overlying framework blocks and debris (red) are deforming the conglomerate body and the basinal sediments

Fig. 9 a Outcrop view of a framework block deforming the distal reef-slope deposits of CB 2; **b** facies interpretation of the outcrop view with distal reef-slope deposits of CB 2 (red), conglomerate body (gray) and distal reef-slope deposits of CB 1 (yellow)

Fig. 10 Model showing the development of CB 1 and CB 2: **a** instability and collapse of the reef framework produces rockfalls and sediment gravity flows (SGF). Grain-size distribution reflects the progressive energy decay of these flows along the slope. The sediments in the distal reef slope are reworked by upslope-directed bottom currents (UBC). Hemipelagic rain (HR) occurs at the distal reef slope. **b** Phases of upslope bottom currents alternate with quiet periods (Fig. 7 in box). **c** A sea-level fall exposes CB 1 triggering erosion (E) of CB 1 deposits. Rockfalls are significant. Conglomerates occur at the base of the framework debris. **d** The CB 2 reef grows on top of framework debris reworked from CB 1. The new framework was in a lower position compared to CB 1 reefs. Fallen blocks extend further down slope into a now shallower basin. **e** During CB 2 growth, sediment gravity flows are stronger as reflected by the persistent parallel lamination in distal reef-slope deposits. Fallen reef-framework blocks deformed these distal deposits (Fig. 9 in box)

Table caption

Table 1 Reef-framework and reef-slope facies of Barranco de los Castaños section.

Figure
Click here to download high resolution image

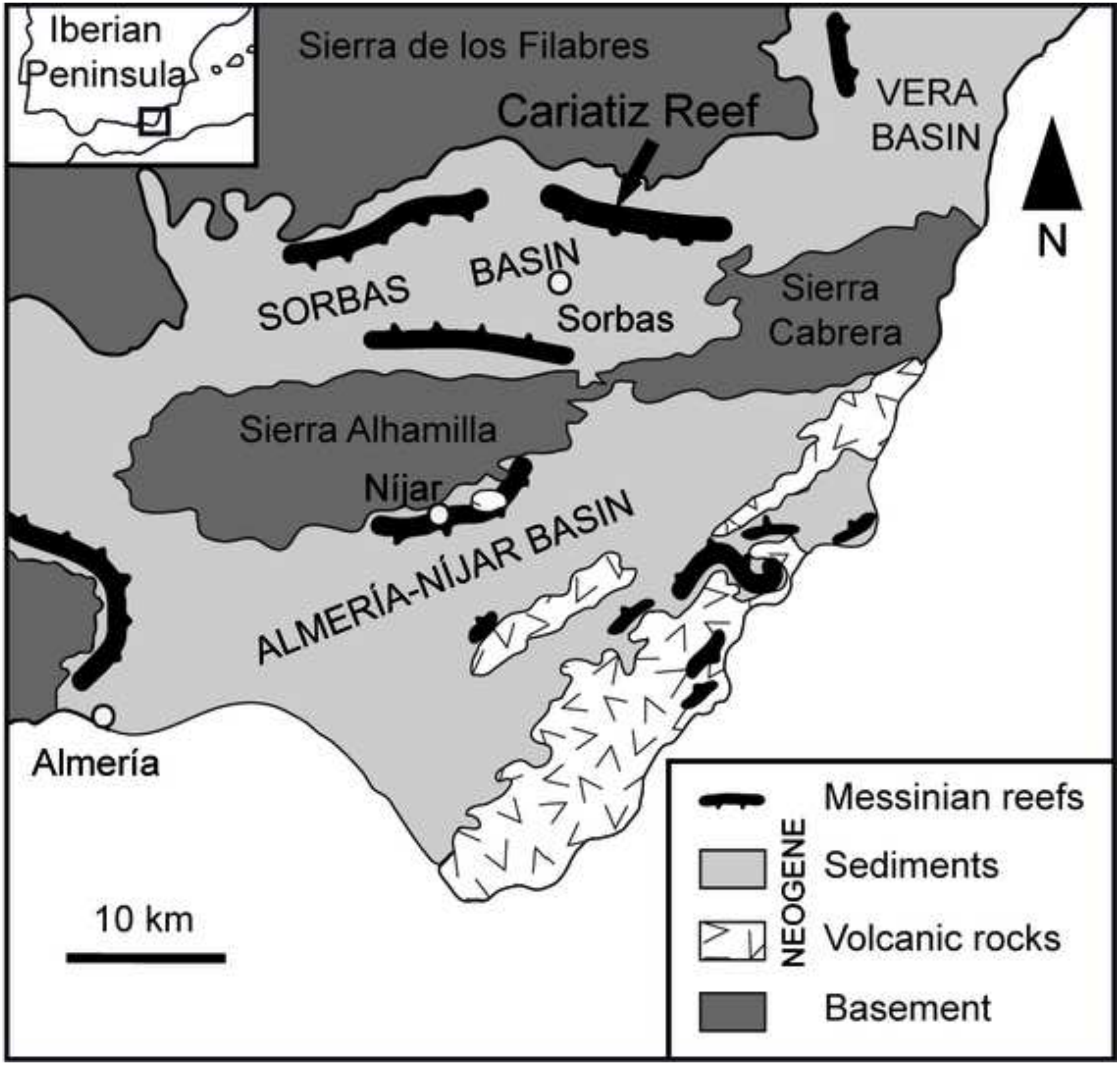

Figure
Click here to download high resolution image

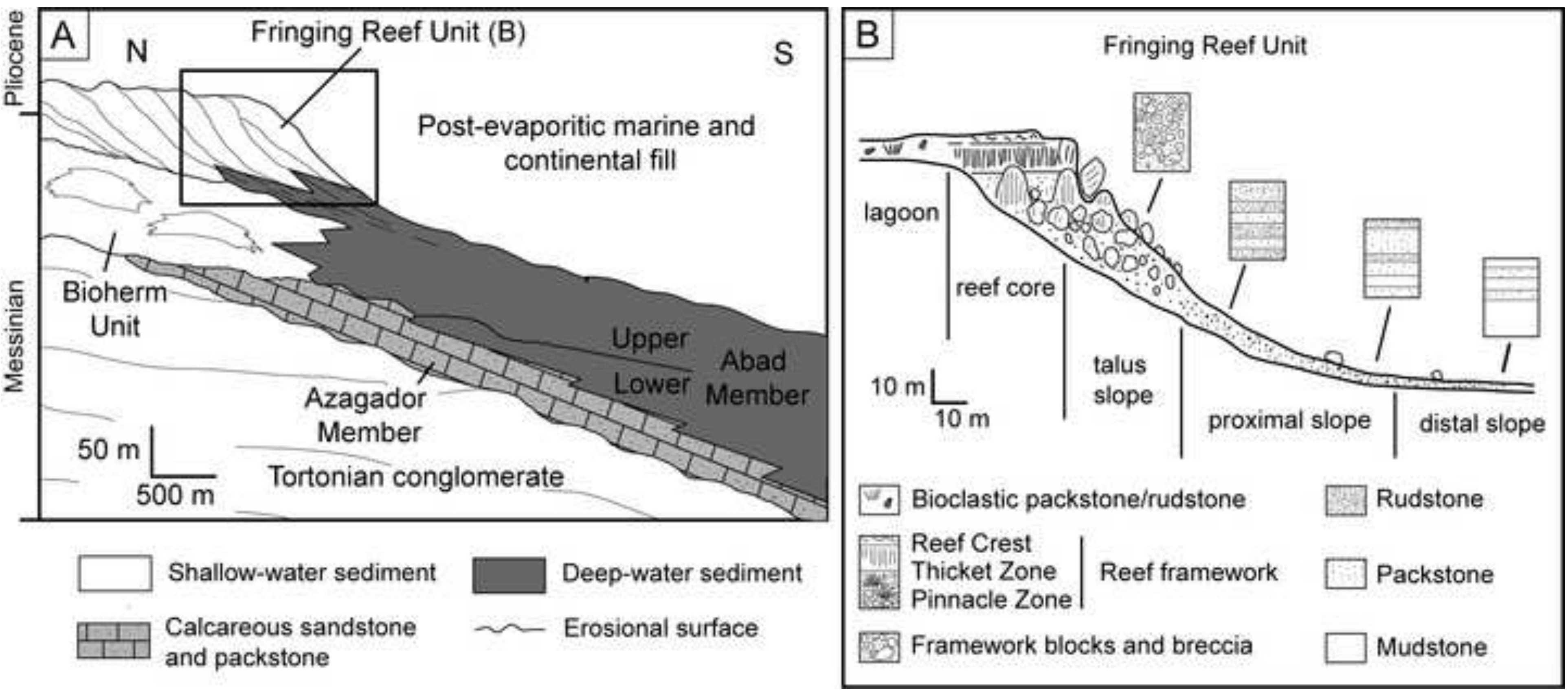

Figure
Click here to download high resolution image

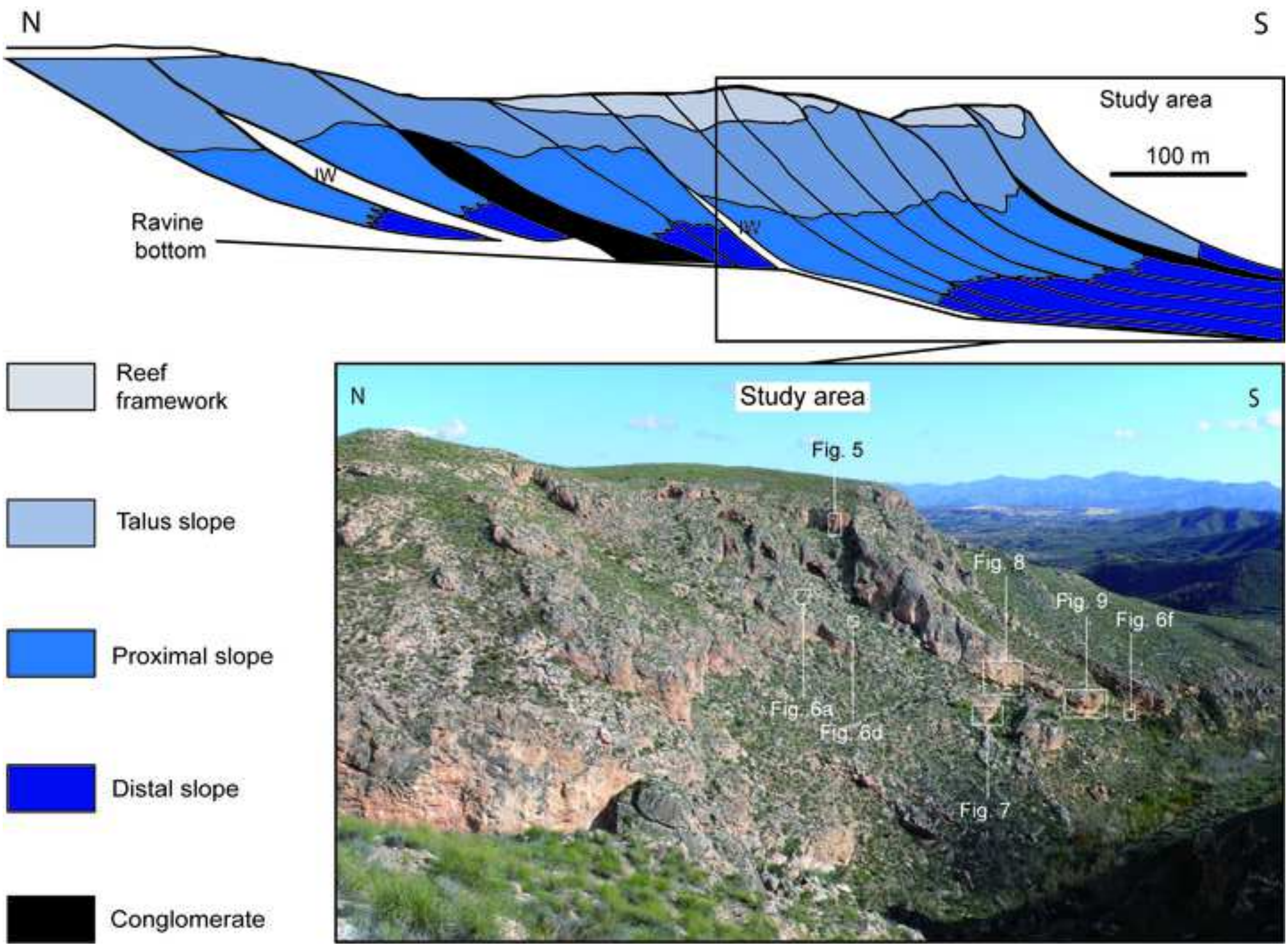

Figure
Click here to download high resolution image

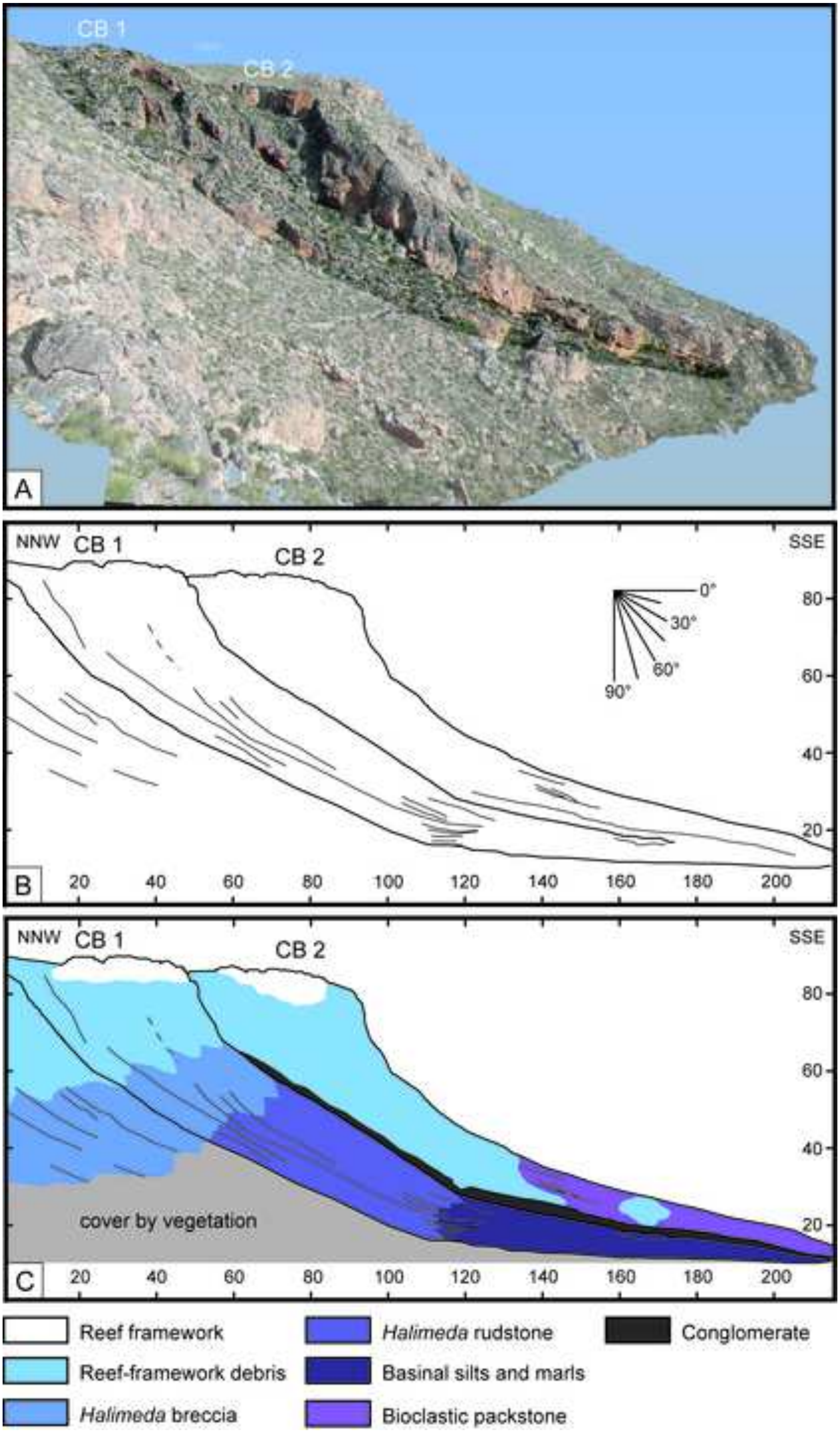

Figure
Click here to download high resolution image

Figure
Click here to download high resolution image

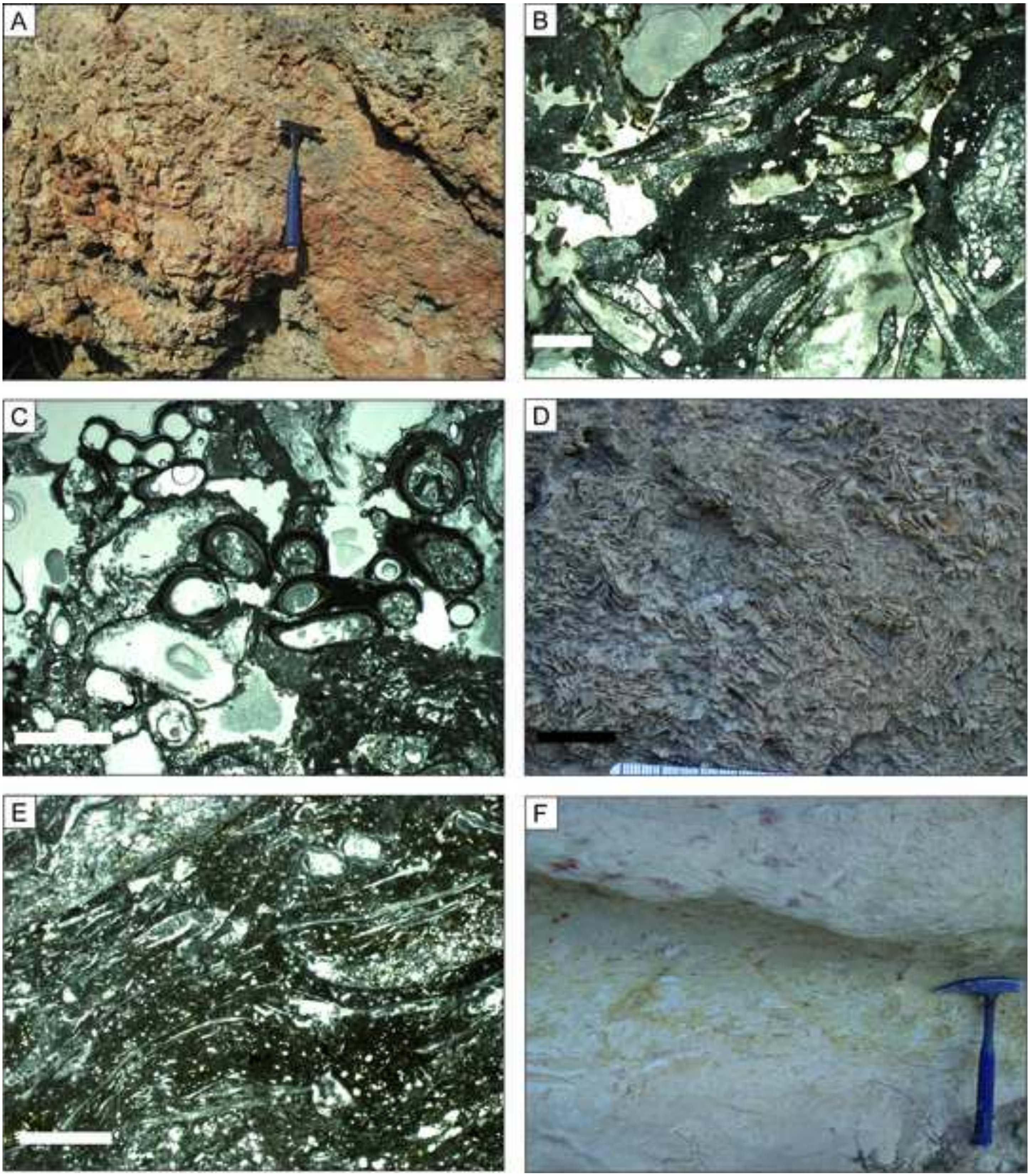

Figure
Click here to download high resolution image

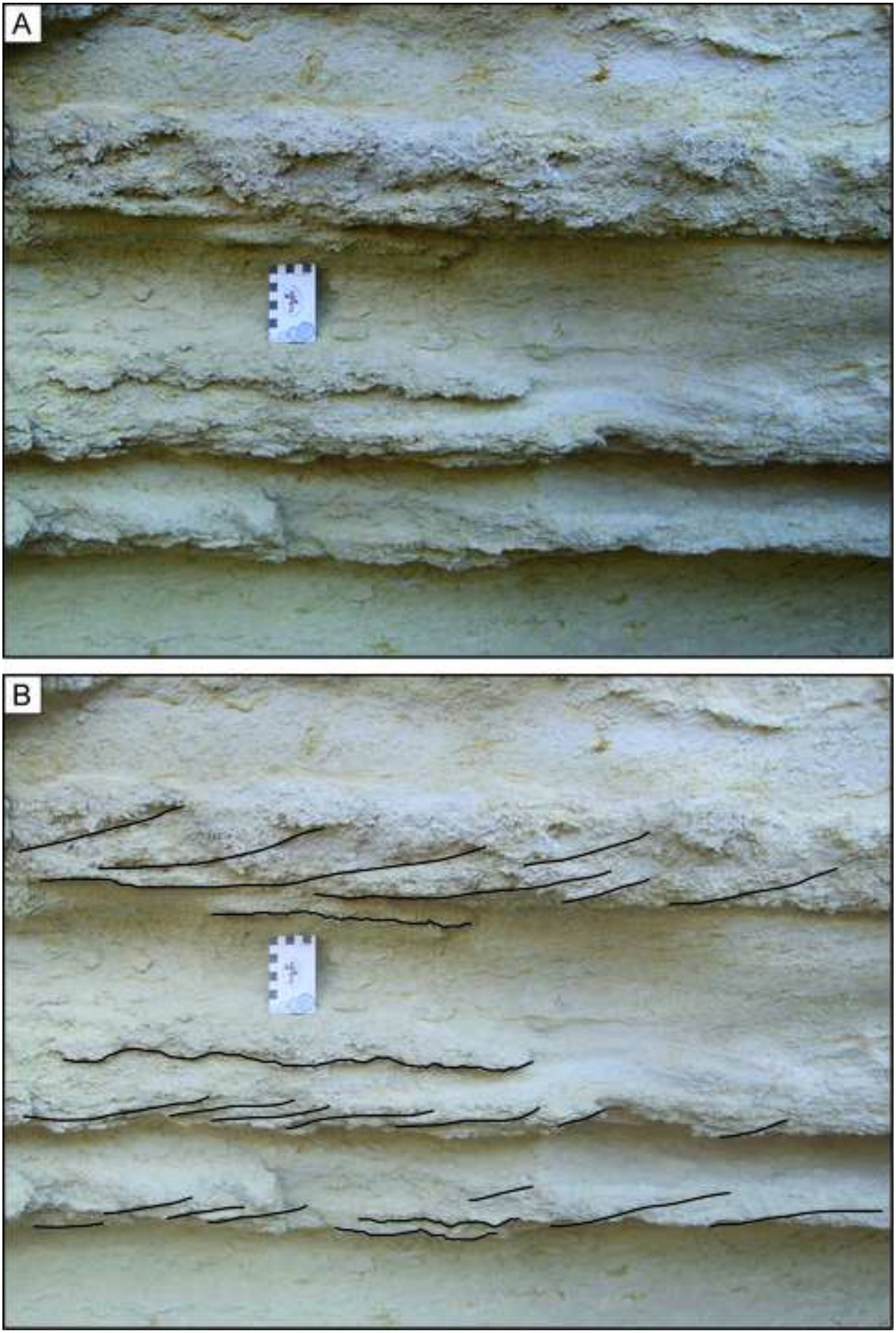

Figure
Click here to download high resolution image

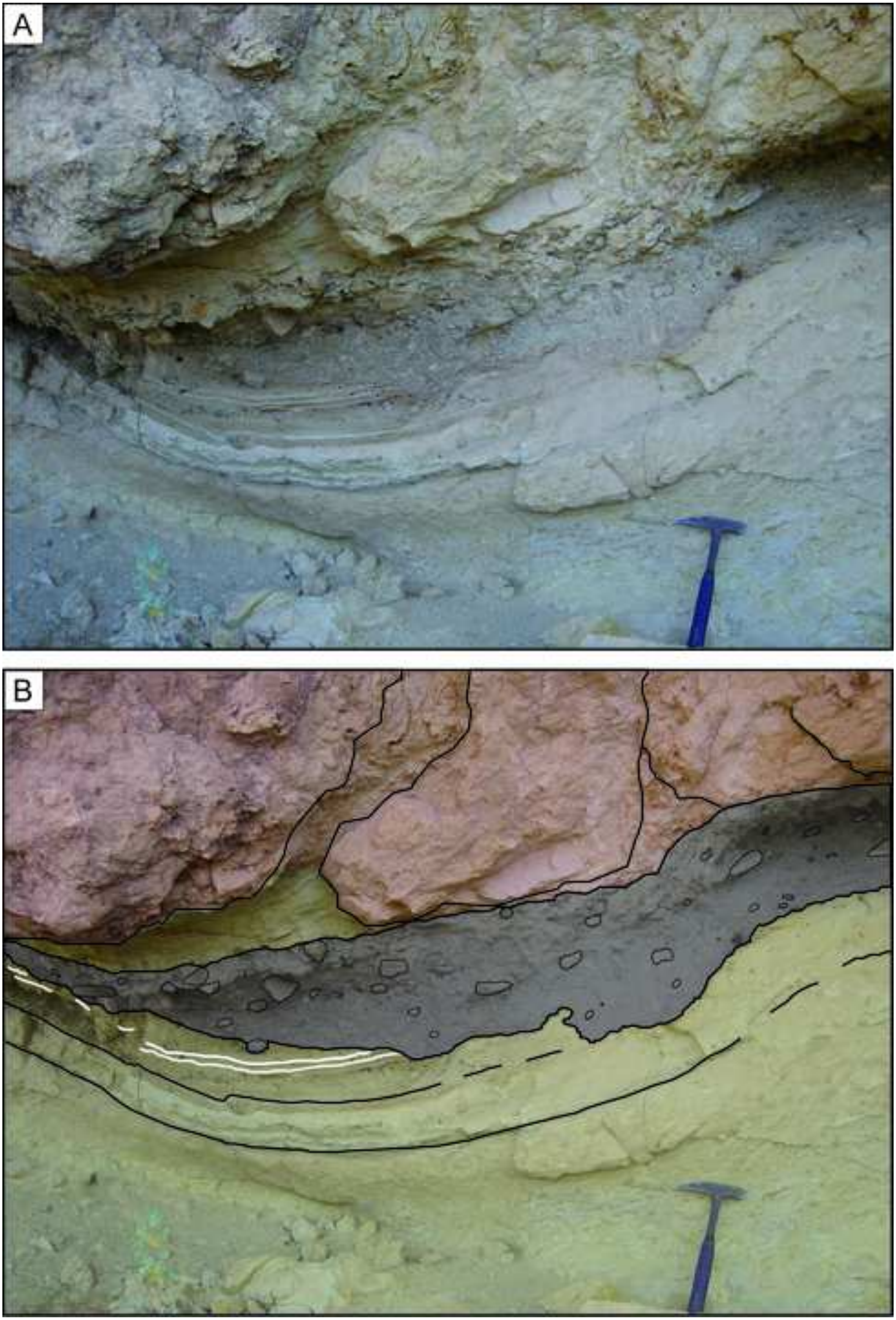

Figure
Click here to download high resolution image

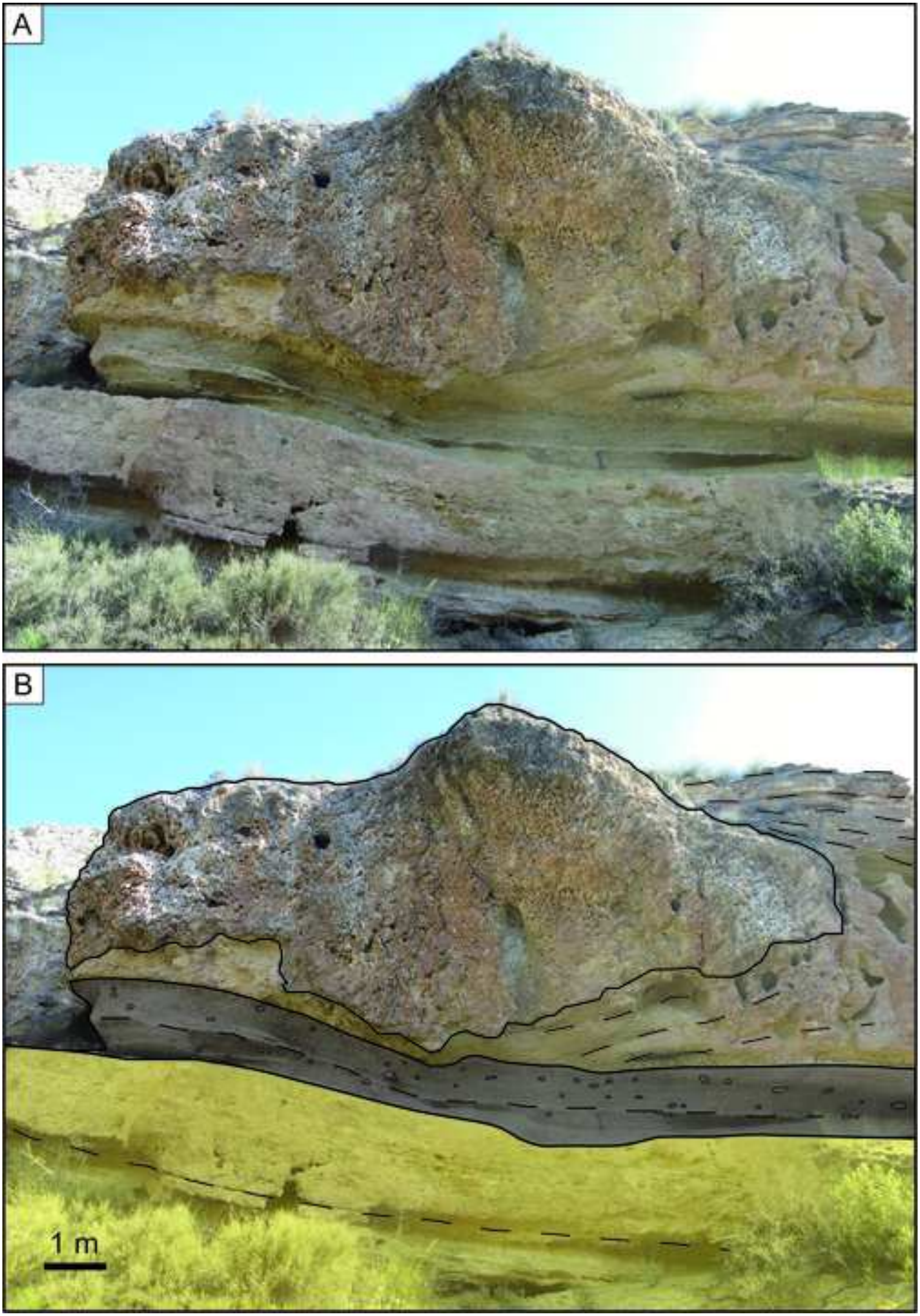

Figure

Click here to download high resolution image

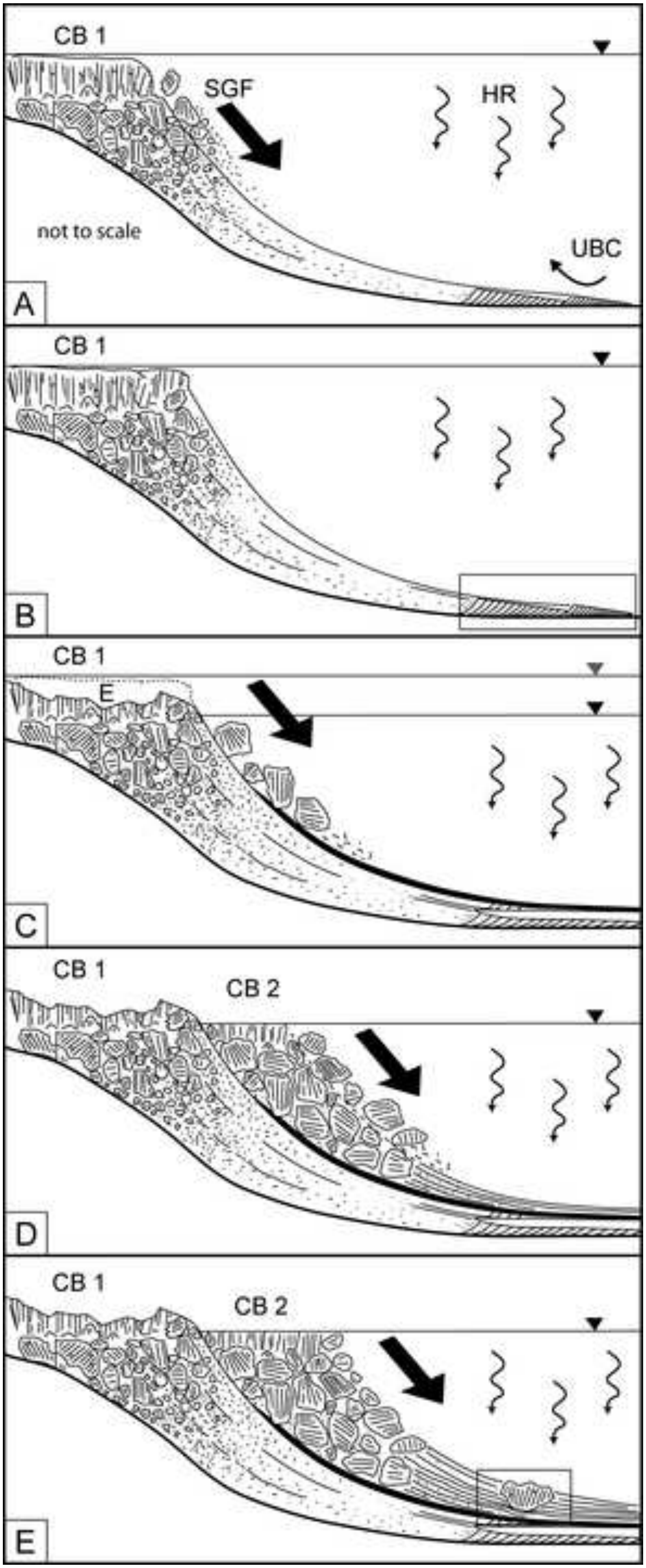

Table

Facies	Components	Matrix	Fabric	Coatings	Position	Dip
Reef-framework (Fig. 5)	*Porites* skeletons (sticks and laminar forms) encrusted by thin coralline algal-foraminiferal coatings covered by thick stromatolitic crusts. Bivalves, echinoids, red algae, brachiopods and gastropods (in gaps).	Microbial (stromatolitic) micrite. Bioclastic matrix.	In situ *Porites* growths. Reef debris (bioclastic rudstone) between *Porites* colonies.	mm-size red algal-foraminiferal coatings. cm- to dm-size stromatolitic crusts.	Platform edge.	--
Reef-framework debris (Fig. 8)	Reef-framework blocks (up to 10 m in size). Echinoids, bivalves (pectinids), brachiopods and gastropods. Intraclasts.	Microgranular (locally microbial micrite matrix).	Chaotic. Poorly bedded in CB 1. Reef-framework block size decrease basinward.	--	Reef-talus slope (CB 1 and CB 2) and proximal reef-slope (CB 2).	60 - 55° CB 1. 80 - 60° (Reef-talus slope CB 2) and 45 - 30° (proximal reef slope CB 2).
Halimeda breccia (Fig. 6a; 6b; 6c) (floatstone to rudstone)	cm-dm reef-framework blocks. *Halimeda* plates. Bivalves (pectinids), gastropods, serpulids, red algae, echinoid spines and benthic foraminifera. Intraclasts and minor siliciclastics.	Microgranular (locally microbial micrite matrix).	Chaotic. Poorly bedded (beds up to 40 cm thick). Local serpulid-red algal patches up to 1 m wide.	Fossils with micritic envelopes, locally connecting bioclasts. Red algal crusts around some bioclasts.	Reef-talus slope (CB 1).	55 - 45° CB 1.
Halimeda rudstone (Fig. 6d)	*Halimeda* plates. Bivalves (pectinids and oysters), gastropods, serpulids and red algae.	Microbial micrite matrix.	5-30 cm thick beds. Bioturbation. In the upper proximal slope 15-25 mm thick red algal nodule beds. In the lower proximal slope low-angle cross-lammination (5 cm high and 20 cm long sets).	Micritic envelopes.	Proximal reef-slope (CB 1).	35 - 30° CB 1.
Bioclastic packstone (Fig. 6e)	Bivalves (pectinids), gastropods, serpulids, benthic foraminifera, red algae and echinoid spines. Siliciclastic grains (7-10%).	Microbial micrite matrix.	10 - 30 cm thick beds with 1-5 cm thick layers. Bivalve shells parallel to bedding (equal concave/convex-up orientation). Locally intercalated with basinal silts and marls.	Micritic envelopes with a major development on one side of the grain (no preferred orientation).	Distal reef-slope (CB 2).	20 - 15° CB 2.
Basinal siltstone and marl (Fig. 6f)	Red algae. Diatoms.	Silts and marls.	15-35 cm thick beds thickening upward to 40-60 cm thick beds. Alternation of mm-cm diatomite beds. Significant bioturbation.	--	Distal reef-slope (CB 1 and CB 2).	15 - 10° CB 1. 20 - 15° CB 2.